Japanese Journal of Applied Physics **54**, 08KD17 (2015) **REGULAR PAPER**
http://dx.doi.org/10.7567/JJAP.54.08KD17

Two-dimensional simulation of interdigitated back contact silicon heterojunction solar cells having overlapped p/i and n/i a-Si:H layers

Hiroshi Noge[1*], Kimihiko Saito[1], Aiko Sato[1], Tetsuya Kaneko[1,2], and Michio Kondo[1,3*]

[1]*Faculty of Symbolic Systems Science, Fukushima University, Fukushima 960-1296, Japan*
[2]*School of Engineering, Tokai University, Hiratsuka, Kanagawa 259-1292, Japan*
[3]*Fukushima Renewable Energy Institute (FREA), National Institute of Advanced Industrial Science and Technology (AIST), Koriyama, Fukushima 963-0298, Japan*
E-mail: noge.hiroshi@aist.go.jp; michio.kondo@aist.go.jp

Received January 9, 2015; accepted April 24, 2015; published online July 16, 2015

The performance of interdigitated back contact silicon heterojunction solar cells having overlapped p/i and n/i a-Si:H layers on the back has been investigated by two-dimensional simulation in comparison with the conventional cell structure having a gap between p/i and n/i layers. The results show that narrower overlap width leads to higher short circuit current and conversion efficiency, especially for poor heterojunction interface and thinner silicon substrate of the cells in addition to narrower uncovered width of p/i layer by a metal electrode. This is similar to the gap width dependence in the conventional cells, since both overlap and gap act as dead area for diffused excess carriers in the back contacts.
© 2015 The Japan Society of Applied Physics

1. Introduction

Interdigitated back contact silicon heterojunction (IBC-SiHJ) solar cells[1–8] have both advantages of the high open circuit voltage with a small temperature coefficient in a heterojunction scheme[9,10] and no shadowing loss in a back contact structure.[11,12] They are currently drawing big attention among crystalline silicon cells and Panasonic and Sharp have achieved over 25% conversion efficiency.[13,14] One representative structure of back contacts in the literatures consists of interdigitated p or p/i-type and n or n/i-type hydrogenated amorphous silicon (a-Si:H) strip layers on a crystalline Si substrate and gaps covered by passivation layers in between.[15–17] The passivation materials are usually i-type a-Si:H, SiO_2 or SiN_x. This "gap" structure can be formed, for example, by 3 time independent deposition of these layers with at least 2 time masked patterning.[4]

On the other hand, another design whose back contacts consist of interdigitated p/i and n/i a-Si:H strip layers that overlap at the edges can be fabricated with 2 time deposition of pair a-Si:H films and 2 time patterning. In fact, Sharp obtained 25.1% efficiency in this structure.[14] Independently from Sharp, we have been developing this type of IBC-SiHJ cells by the use of inkjet printing for cost reduction.[18] Here we have an advantage in the simplified process, however, there could be the loss in current collection due to the overlap between p/i and n/i layers, whose geometry is affected by the patterning resolution and accuracy. In this paper, we have investigated the optimum cell design of this "overlapped" structure and examined the influence of the overlap width and other dimensions of the back contacts on the cell performance by two-dimensional numerical simulation using SILVACO's ATLAS software in comparison with the "gap" cells.

2. Simulation model

2.1 Cell structure

The unit structure of the IBC-SiHJ cell for simulation assuming the horizontal periodicity is illustrated in Fig. 1. Note that this figure depicts only half of the elementary cell in width. On the front surface of an n-type crystalline silicon (c-Si) substrate, which is illuminated, a single dielectric film whose refractive index is 2.74 and thickness is 100 nm, is coated for antireflection and n- and i-type a-Si:H layers are inserted for front surface field (FSF)[19] and for passivation, respectively. Both thicknesses of the top n- and i-type a-Si:H layers are assumed to be 5 nm. On the back side, the c-Si substrate is partially covered by stacked p/i a-Si:H films for emitter. The remaining back surface is covered by stacked n/i a-Si:H films for back surface field (BSF), which extend on the edges of p/i films with the overlap width of typically 100 μm. The lateral half widths of the p/i a-Si:H film and the n/i a-Si:H film without the overlap, which are defined as W_p and W_n are typically 750 and 150 nm, respectively. The thickness of the back i-type a-Si:H film is 5 nm and both thicknesses of the back p- and n-type a-Si:H layers are 5 nm. In practice, the p/i and n/i strip layers are arranged in an interdigitated manner on a substrate plane. They are covered by metal electrodes for contacts with the uncovered width of typically 100 μm, preventing the leakage even by the rough patterning process. The thickness of the substrate is typically 100 μm. Both surfaces of the substrates are flat, namely have no textures for the convenience of calculation, sacrificing the enhancement of photo generation current by optical confinement. 100% reflection of the penetrating light on the back by an ideal reflector is assumed. The typical dimensions

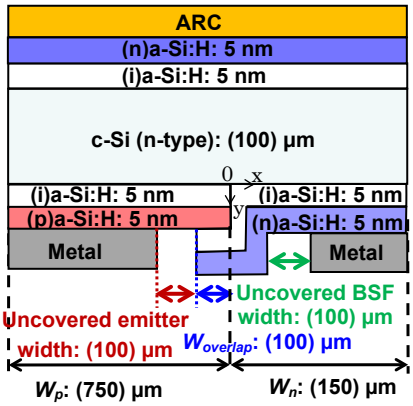

Fig. 1. (Color online) Cell unit model of the overlapped structure for simulation. Numbers in ( ) are default dimensions. ARC stands for antireflection coating film. The x–y coordinate corresponds to the axes in Figs. 2 and 3 whereas the dimensions are not in scale.

© 2015 The Japan Society of Applied Physics

Table I. Defect state parameters of a-Si:H for simulation.

		n-type a-Si:H	i-type a-Si:H	p-type a-Si:H
Conduction tail states	Density (cm^{-3})	10^{21}	10^{18}	10^{21}
	Width (eV)	0.07	0.06	0.07
	Electron capture cross-section (cm^2)	2×10^{-16}	2×10^{-16}	2×10^{-16}
	Hole capture cross-section (cm^2)	1×10^{-16}	1×10^{-16}	1×10^{-16}
Valence tail states	Density (cm^{-3})	10^{21}	10^{18}	10^{21}
	Width (eV)	0.12	0.09	0.12
	Electron capture cross-section (cm^2)	1×10^{-16}	1×10^{-16}	1×10^{-16}
	Hole capture cross-section (cm^2)	3×10^{-17}	3×10^{-17}	3×10^{-17}
Acceptor-like mid-gap states	Density (cm^{-3})	10^{19}	10^{16}	10^{19}
	Energy position (eV)	0.7	1.1	1.3
	Width (eV)	0.2	0.15	0.2
	Electron capture cross-section (cm^2)	1×10^{-16}	1×10^{-16}	1×10^{-16}
	Hole capture cross-section (cm^2)	1×10^{-16}	1×10^{-16}	1×10^{-16}
Donor-like mid-gap states	Density (cm^{-3})	10^{19}	10^{16}	10^{19}
	Energy position (eV)	0.45	0.9	1.1
	Width (eV)	0.2	0.15	0.2
	Electron capture cross-section (cm^2)	5×10^{-17}	5×10^{-17}	5×10^{-17}
	Hole capture cross-section (cm^2)	1×10^{-15}	1×10^{-15}	1×10^{-15}

are varied when their influence on the cell performance is examined.

For comparison, a "gap" structure cell with almost the same dimensions as the "overlapped" structure is also simulated. In this structure, n/i and p/i overlapped layers are replaced with a bare c-Si surface having the designated surface recombination velocity.

2.2 Physical models and parameters

300 K bandgaps of c-Si and a-Si:H are assumed to be 1.08 and 1.75 eV, respectively and their electron affinities are 4.17 and 3.82 eV, respectively assuming Anderson model at the heterojunction in ATLAS.[17,20,21] The doping concentrations of c-Si and i-type, p-type, front n-type, and back n-type a-Si:H are 2×10^{16}, 1×10^{15}, 5×10^{18}, 1×10^{18}, and $8 \times 10^{18}\,cm^{-3}$, respectively.

For c-Si material, the bulk lifetime is set to be 5 ms and Shockley–Read–Hall[22,23] and Auger recombination[24,25] models are applied and the carrier concentration dependent mobility[26] is considered in ATLAS.[21] For a-Si:H, the effective density of states of both conduction and valence bands at 300 K is set to be $2 \times 10^{20}\,cm^{-3}$ and the mobilities of electrons and holes are 5 and $0.3\,cm^2\,V^{-1}\,s^{-1}$,[27] respectively. The defect states of a-Si:H is modeled by two (conduction and valence) exponentially decaying band tail states and two (one acceptor-like and the other donor-like) Gaussian distribution mid-gap states[28] using TFT module of ATLAS.[21] The densities and the widths of tail and gap states and the energy position of the gap states are taken from Ref. 15 and are summarized in Table I. Their capture cross sections for electrons and holes are also listed in the same table.

For realistic modeling of c-Si/a-Si:H heterojunction, thin (1 nm) defective layer of c-Si is inserted at the interface.[17,29] The Gaussian distribution defect states are located at center of the gap and the width of them is set to be 0.2 eV. Their capture cross section for both electrons and holes are $10^{-16}\,cm^2$. The default defect density, N_{int} is $1.41 \times 10^{18}\,cm^{-3}$. The thermoionic emission and Fowler–Nordheim tunneling are modeled for the carrier transport at the heterojunction in ATLAS. The quantum confinement effect[30] is not considered for simplicity since our interest is on the optimization of lateral dimensions of the cell structure.

In simulation, photo generation rate under AM1.5G illumination was firstly calculated by ray tracing method. The default ATLAS data base was used for optical constants. Then, the electrical calculations based on the drift-diffusion model using Boltzmann statistics were carried out with varying the applied voltage to obtain the cell performance.

3. Results and discussion

3.1 Electric field and current distribution

The basic operation of "overlapped" structure cell is almost the same as that of a conventional "gap" structure. Most of excess carriers are generated near the front surface and diffuse in the substrate. Then a part of them that survive without the recombination and arrive in the vicinity of the back contacts is attracted into the contacts by the local electric fields. The difference between the overlapped and gap structures lies in the overlap or gap regions.

The distribution contour maps of the electric field and the current density for the typical overlapped structure are illustrated in Figs. 2 and 3, respectively. The maps for the corresponding gap structure are also shown for comparison. The electric field above the overlap is almost cancelled out in the n/i/p junction and results in very small current flow as in the gap region of the gap structure where no electrical contact is placed. This fact suggests that the similar performance of the overlapped cell is expected to that of the gap cell when they have the similar quality of the back surface in the overlap or the gap regions as discussed later.

3.2 Influence of emitter and BSF widths

In order to optimize the rear geometry of the overlapped cell, the influence of the half emitter (p/i a-Si:H layer) width, W_p

© 2015 The Japan Society of Applied Physics

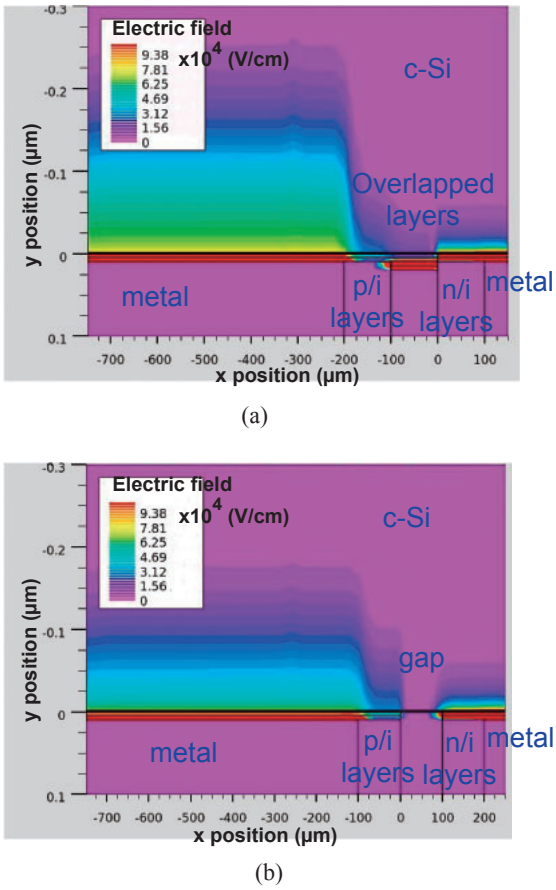

Fig. 2. (Color) Contour color maps of electric field distribution in linear scale near the back contact at 0 V (a) for the overlapped structure and (b) for the gap structure. The vertical scale is exaggerated.

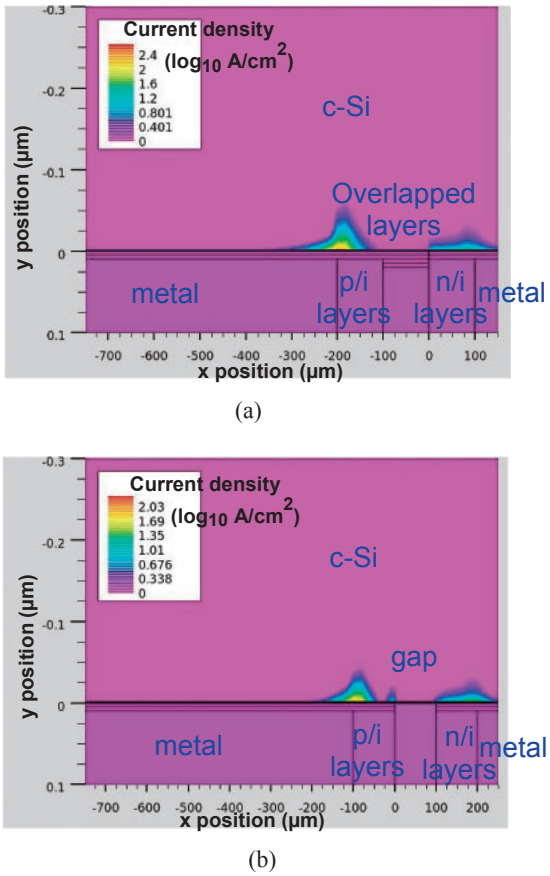

Fig. 3. (Color) Contour color maps of current density distribution in logarithmic scale near the back contact at 0 V (a) for the overlapped structure and (b) for the gap structure. The vertical scale is exaggerated.

or the half BSF (n/i a-Si:H layer without the overlap) width, W_n was studied while holding the other parameters constant. The calculated short circuit current density (J_{SC}) and conversion efficiency (η) are plotted as a function of W_p or W_n in Fig. 4. The open circuit voltage (V_{OC}) and fill factor (FF) do not change largely in the range between 0.70–0.73 V and 0.797–0.81, respectively. With the increase of W_p or with the decrease of W_n, J_{SC} and η are improved to the extent of the calculated parameter range. The minority carriers (holes) generated in the substrate above the emitter are efficiently transported to the emitter with small lateral motion for wider W_p as long as their travelling distance is much shorter than their diffusion length. On the other hand, those generated above the BSF are required to move longer distance to reach the emitter for wider W_n. This explains the dependence of J_{SC} and eventually η on the emitter and BSF widths.

The above characteristics in the overlapped structure are completely the same as in the gap structure. Judging from these results, rough resolution around 100 μm is allowed for pattering the emitter and BSF layers since W_p and W_n are the half of the actual strip widths.

3.3 Influence of overlap width and interface defect density in comparison with the gap structure

Most important dimension of the back contact in the overlapped structure cell is the overlap width, $W_{overlap}$ between n/i and p/i a-Si:H layers. By the existence of an overlap, the minority carriers generated above the BSF need to travel longer laterally for the emitter and in addition, the recombination probability is enhanced in the overlap region especially for highly defective heterointerface. Figure 5 shows the V_{OC}, J_{SC}, FF, and η as a function of $W_{overlap}$ for different interface defect densities in the 1 nm defective layer. When $N_{int} = 1.41 \times 10^{17}\,cm^{-3}$, namely the areal interface defect density, $D_{int} = 1.41 \times 10^{10}\,cm^{-2}$, the cell performance does not degrade significantly even with large $W_{overlap}$. However, for higher defect densities, all V_{OC}, FF, and especially J_{SC} and eventually η drop rapidly with the increase of overlap width because the overlapped interfaces act as dead areas for the photo generated excess carriers. In addition, even at zero overlap width, these performance characteristics are degraded due to the intensive recombination at the whole back heterointerfaces.

For comparison, the cell performance of the corresponding gap structure having the different surface recombination velocities, S_{gap} at the gap was also simulated. The calculated V_{OC}, J_{SC}, FF, and η are plotted as a function of the gap width, W_{gap} in Fig. 6. These characteristic values are the same for the different S_{gap} at $W_{gap} = 0$, because the defect density at the heterointerface of the emitter and the BSF is unchanged. As for the gap width dependency, when $S_{gap} \leq 100$ cm/s, the cell performance does not degrade significantly even with large W_{gap}, However, similarly to the overlapped structure, all V_{OC}, FF, J_{SC}, and η drop rapidly with the increase of gap width for larger S_{gap}. The relationship between the interface defect density, N_{SS} and the surface recombination velocity,

© 2015 The Japan Society of Applied Physics

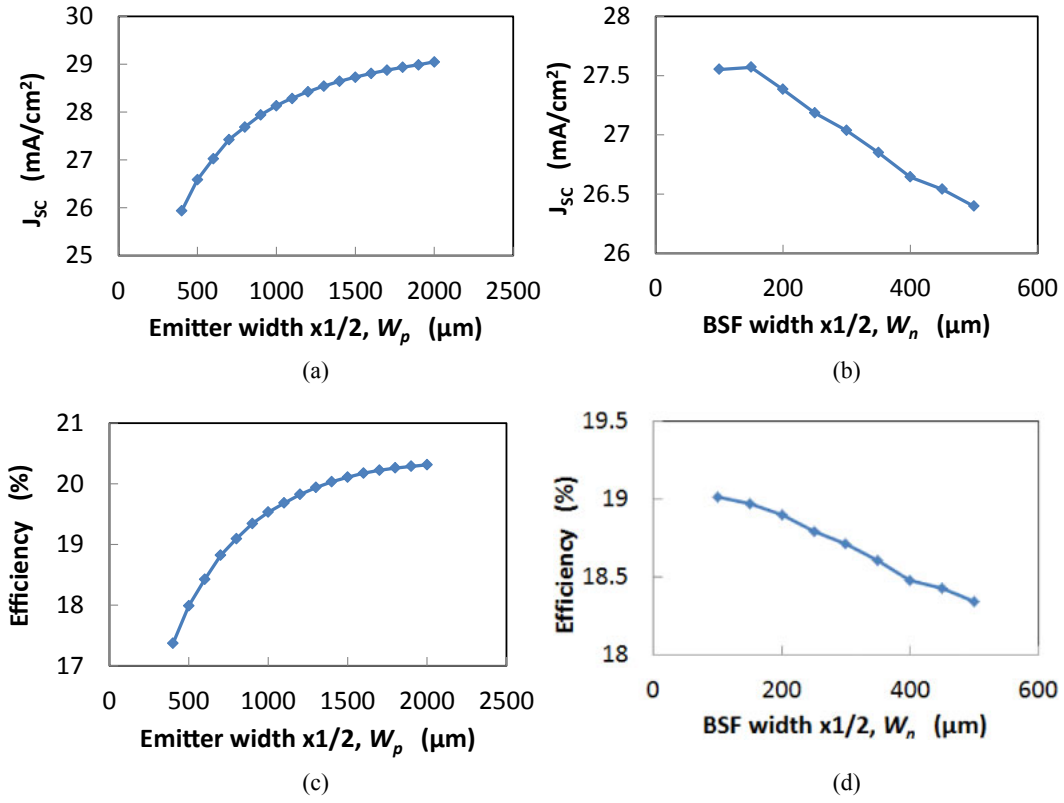

Fig. 4. (Color online) (a, b) Short circuit current density, J_{SC} and (c, d) conversion efficiency, η as a function of (a, c) the half of emitter (p layer) width, W_p and (b, d) the half of BSF (n layer) width, W_n.

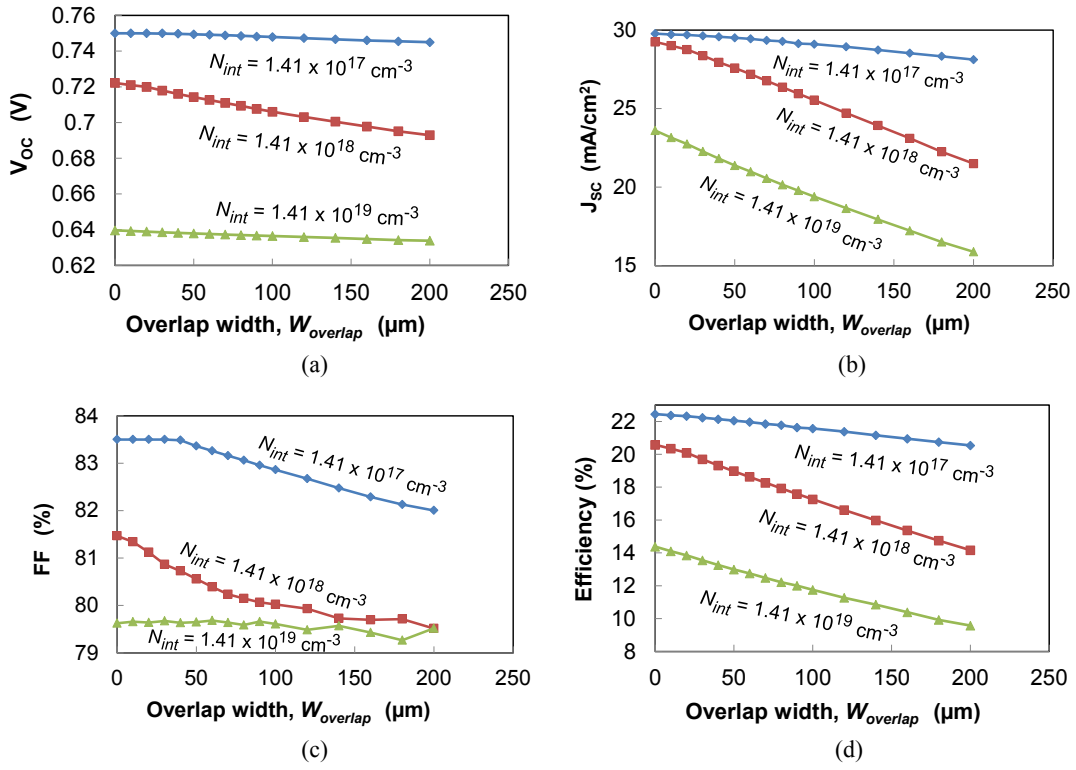

Fig. 5. (Color online) (a) Open circuit voltage, V_{OC}, (b) short circuit current density, J_{SC}, (c) fill factor, FF, and (d) conversion efficiency, η of the overlapped structure as a function of overlap width, $W_{overlap}$ for various heterointerface defect densities, N_{int}.

SRV for the front c-Si/a-Si:H heterointerface of the gap structure has been discussed and the linear relation: *SRV* (cm/s) = $13 + 6.7 \times 10^{-11}$ N_{SS} (cm^{-2}) has been found.[19] This cannot be directly applied to our case since we are discussing the relationship between the different structures and the different distribution of interface defects, however,

© 2015 The Japan Society of Applied Physics

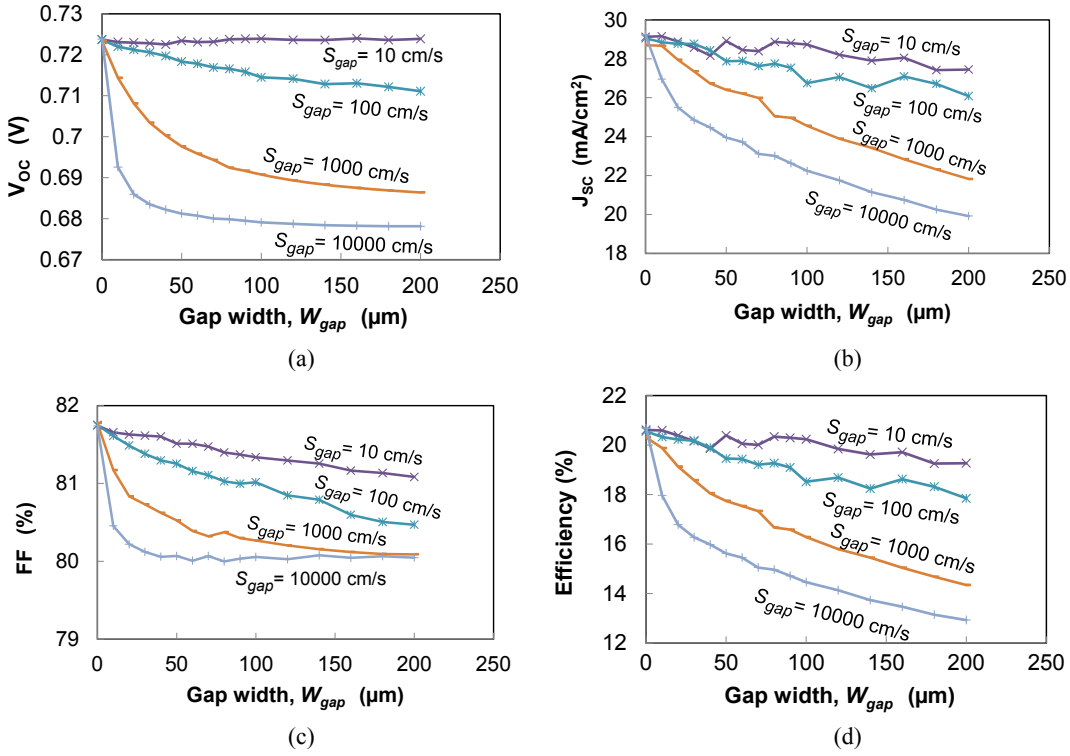

Fig. 6. (Color online) (a) Open circuit voltage, V_{OC}, (b) short circuit current density, J_{SC}, (c) fill factor, FF, and (d) conversion efficiency, η of the gap structure as a function of gap width, W_{gap} for various surface recombination velocities, S_{gap}.

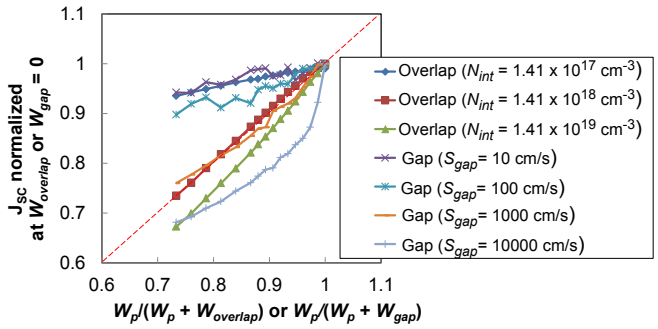

Fig. 7. (Color online) J_{SC} of the overlapped and gap structures normalized at $W_{overlap}$ or $W_{gap} = 0$ as a function of the ratio of effective emitter width, $W_p/(W_p + W_{overlap})$ or $W_p/(W_p + W_{gap})$. Dashed line is a guide for eyes indicating that J_{SC} is proportional to the ratio of effective emitter width.

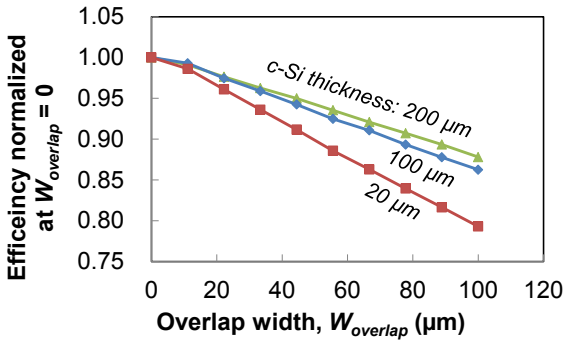

Fig. 8. (Color online) Conversion efficiency dependence of the overlapped structure on overlap width, $W_{overlap}$ for various c-Si substrate thicknesses. The efficiency is normalized at $W_{overlap} = 0$.

we can see the resembled correlation in Figs. 5 and 6 when looking at the relative dependence on the overlap and gap widths.

For poor heterointerface in the overlapped structure or for defective gap surface in the gap structure, the overlap or the gap acts as a dead area and would practically reduce the emitter width and consequently the current almost proportionally to its reduction ratio. Figure 7 shows the normalized J_{SC} at $W_{overlap}$ or $W_{gap} = 0$ as a function of the width ratio of W_p to $(W_p + W_{overlap})$ or $(W_p + W_{gap})$. The decrease of J_{SC} is roughly proportional to the undead ratio of emitter width for heavily defective heterointerfaces or gap surfaces.

3.4 Influence of substrate thickness

Recently, a c-Si substrate for solar cells becomes thinner aiming at the cost saving and the enhancement of V_{OC} in spite of reduced J_{SC}. We examined the influence of c-Si thickness on the cell performance in the overlapped structure. Conversion efficiencies normalized at $W_{overlap} = 0$ are plotted as a function of overlap width for the different substrate thicknesses, 200, 100, and 20 μm in Fig. 8. Influence of the overlap width becomes more significant for thinner substrate whose thickness is comparable or less than the overlap width probably because the excess carriers are more likely to recombine in the overlap region in their lateral motion in thinner substrate.

3.5 Influence of uncovered widths by metal electrodes

In addition to the overlap width, the widths of the emitter and BSF area uncovered by metal electrodes, in turn the metal coverages are also important for the cell performance as have been investigated for the gap structure cells.[31] Figure 9 is the calculated result of conversion efficiencies normalized at $W_{overlap} = 0$ as a function of uncovered width on emitter and

© 2015 The Japan Society of Applied Physics

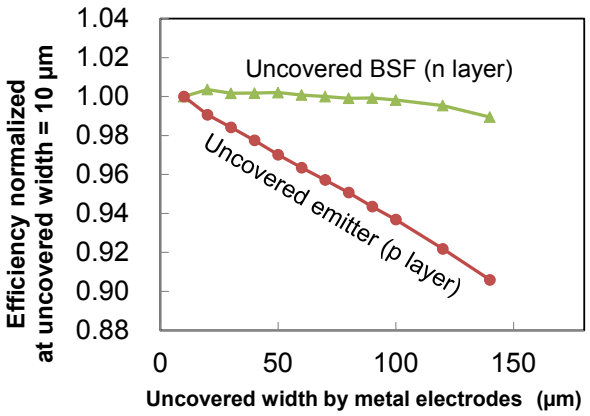

Fig. 9. (Color online) Conversion efficiency dependence of the overlapped structure on uncovered emitter or BSF width by metal electrodes. The efficiency is normalized at the width of 10 μm.

BSF. While the uncovered width on the BSF n/i layer does not largely influence on the efficiency, it is remarkably deteriorated with the increase of that on the emitter p/i layer. It can be considered that when the resistivity of the p-type a-Si:H layer is relatively high, the surface potential of c-Si on the uncovered area by a metal electrode drops and the formation of an inversion layer which carries the current dominantly in this area is suppressed. Therefore, wider uncovered width of the p/i layer results in lower J_{SC} and efficiency. This should be also affected by the doping density and the thickness of the p layer. On the other hand, the low resistivity of the n-type a-Si:H layer does not influence the formation of an accumulation layer in the uncovered area by a metal electrode significantly and hence, the dependence on the uncovered width is small on the n/i layer. Roughly speaking, the accuracy less than 50 μm is preferable in the patterning that defines the metal coverage as well as the overlap width.

4. Conclusions

We have studied the performance of IBC-SiHJ solar cells having overlapped p/i and n/i a-Si:H layers on the back by two-dimensional simulation in comparison with the conventional cells having a gap between p and n layers. The overlap width should be as narrow as possible for better J_{SC} and efficiency, especially for the poor heterojunction interface and thinner c-Si substrate of the cells as the gap width in the gap structures, since they act as dead areas for excess carriers. In addition, narrower uncovered width of the relatively high resistivity p layer by a metal electrode is also important for larger J_{SC} and efficiency in the patterning of back contacts.

Acknowledgments

The authors acknowledge FREA and Research Center for Photovoltaic Technologies (RCPVT) of AIST for the experimental facilities. This work was supported by Ministry of Education, Culture, Sports, Science and Technology of Japan (MEXT) in Fukushima Regional Innovation Strategy Promotion Program.

1) M. Lu, S. Bowden, U. Das, and R. Birkmire, Appl. Phys. Lett. **91**, 063507 (2007).
2) R. Stangl, J. Haschke, M. Bivour, M. Schmidt, K. Lips, and B. Rech, Proc. 33rd IEEE Photovoltaic Specialists Conf. (PVSC), 2008, p. 1.
3) R. Stangl, J. Haschke, M. Bivour, L. Korte, M. Schmidt, K. Lips, and B. Rech, Sol. Energy Mater. Sol. Cells **93**, 1900 (2009).
4) M. Tucci, L. Serenelli, E. Salza, L. Pirozzi, G. de Cesare, D. Caputo, M. Ceccarelli, P. Martufi, S. De Iullis, and L. J. Geerlings, Proc. 23rd European Photovoltaic Solar Energy Conf. (EU-PVSEC), 2008, p. 1749.
5) T. Desrues, P.-J. Ribeyron, A. Vandeneynde, A.-S. Ozanne, D. Muñoz, F. Souche, C. Denis, D. Heslinga, D. Diouf, and J. P. Kleider, Proc. 24th European Photovoltaic Solar Energy Conf. (EU-PVSEC), 2009, p. 2202.
6) T. Desrues, F. Souche, A. Vandeneynde, D. Muñoz, A.-S. Ozanne, and P. J. Ribeyron, Proc. 25th European Photovoltaic Solar Energy Conf. (EU-PVSEC), 2010, p. 2374.
7) A. Hertanto, H. Liu, D. Yeghikyan, B. G. Rayaprol, N. P. Kherani, and S. Zukotynski, Proc. 34th IEEE Photovoltaic Specialists Conf. (PVSC), 2009, p. 1767.
8) B. J. O'Sullivan, T. Bearda, Y. Qiu, J. Robbelein, C. Gong, N. E. Posthuma, I. Gordon, and J. Poortmans, Proc. 35th IEEE Photovoltaic Specialists Conf. (PVSC), 2010, p. 3549.
9) M. Tanaka, M. Taguchi, T. Matsuyama, T. Sawada, S. Tsuda, S. Nakano, H. Hanafusa, and Y. Kuwano, Jpn. J. Appl. Phys. **31**, 3518 (1992).
10) T. Mishima, M. Taguchi, H. Sakata, and E. Maruyama, Sol. Energy Mater. Sol. Cells **95**, 18 (2011).
11) E. Van Kerschaver and G. Beaucarne, Prog. Photovoltaics **14**, 107 (2006).
12) P. J. Cousins, D. D. Smith, H.-C. Luan, J. Manning, T. D. Dennis, A. Waldhauer, K. E. Wilson, G. Harley, and W. P. Mulligan, Proc. 35th IEEE Photovoltaic Specialists Conf. (PVSC), 2010, p. 275.
13) K. Masuko, M. Shigematsu, T. Hashiguchi, D. Fujishima, M. Kai, N. Yoshimura, T. Yamaguchi, Y. Ichihashi, T. Mishima, N. Matsubara, T. Yamanishi, T. Takahama, M. Taguchi, E. Maruyama, and S. Okamoto, IEEE J. Photovoltaics **4**, 1433 (2014).
14) J. Nakamura, N. Asano, T. Hieda, C. Okamoto, H. Katayama, and K. Nakamura, IEEE J. Photovoltaics **4**, 1491 (2014).
15) M. Lu, U. Das, S. Bowden, S. Hegedus, and R. Birkmire, Prog. Photovoltaics **19**, 326 (2011).
16) D. Diouf, J. P. Kleider, T. Desrues, and P.-J. Ribeyron, Mater. Sci. Eng. B **159–160**, 291 (2009).
17) D. Diouf, J.-P. Kleider, and C. Longeaud, in *Physics and Technology of Amorphous–Crystalline Heterostructure Silicon Solar Cells*, ed. W. G. J. H. M. van Sark and K. Roca (Springer, Berlin, 2012) Chap. 15.
18) K. Saito, H. Noge, A. Sato, T. Kaneko, and M. Kondo, Proc. 29th European Photovoltaic Solar Energy Conf. (EU-PVSEC), 2014, p. 1249.
19) D. Diouf, J. P. Kleider, T. Desrues, and P.-J. Ribeyron, Energy Procedia **2**, 59 (2010).
20) R. L. Anderson, Solid-State Electron. **5**, 341 (1962).
21) User's manual for ATLAS version 5.19.20.R (Silvaco Inc.).
22) W. Shockley and W. T. Read, Phys. Rev. **87**, 835 (1952).
23) R. N. Hall, Phys. Rev. **87**, 387 (1952).
24) J. G. Fossum and D. S. Lee, Solid-State Electron. **25**, 741 (1982).
25) M. J. Kerr and A. Cuevas, J. Appl. Phys. **91**, 2473 (2002).
26) G. Masetti, M. Severi, and S. Solmi, IEEE Trans. Electron Devices **30**, 764 (1983).
27) K. Zhu, J. Yang, W. Wang, E. A. Schiff, J. Liang, and S. Guha, MRS Proc. **762**, 297 (2003).
28) M. F. Thorpe and D. Weaire, Phys. Rev. Lett. **27**, 1581 (1971).
29) A. S. Gudovskikh, S. Ibrahim, J. P. Kleider, J. Damon-Lacoste, P. Roca i Cabarrocas, Y. Veschetti, and P.-J. Ribeyron, Thin Solid Films **515**, 7481 (2007).
30) Y. Hayashi, D. Li, A. Ogura, and Y. Ohshita, IEEE J. Photovoltaics **3**, 1149 (2013).
31) J. Haschke, Y.-Y. Chen, R. Gogolin, M. Mews, N. Mingirulli, L. Korte, and B. Rech, Energy Procedia **38**, 732 (2013).

© 2015 The Japan Society of Applied Physics